

Geometric Dependence of Fracture Criteria in AL2024

S.J. Lewis^{1,a}, M. Mostafavi^{1,b}, M.J. Pavier^{1,c}, D.J. Smith^{1,d} and C.E. Truman^{1,e}

¹Dept. of Mechanical Engineering, University of Bristol,
Queens Building, University Walk, Bristol, BS8 1TR, U.K.

^asimon.lewis@bristol.ac.uk, ^bm.mostafavi@bristol.ac.uk, ^cmartyn.pavier@bristol.ac.uk,
^ddavid.smith@bristol.ac.uk, ^ec.e.truman@bristol.ac.uk

Keywords: Fracture, Aluminium, J integral, local approach, hydrostatic stress, energy

Abstract. The failure by tensile fracture of a 2024 aluminium alloy was investigated using a number of fracture criteria. The J integral method was shown to exhibit a significant dependency on specimen geometry and was therefore deemed unsuitable for use across a broad range of specimen types. Three ‘local approach’ criteria were also employed, the standard Beremin type model based on maximum principal stress and hydrostatic stress, as well as an alternative method based on dilatational strain energy density. All three models were found to be capable of characterizing the failure behaviour of the material in question, although it was noted that the results of the Beremin method were highly sensitive to the data used to calibrate the model. The energy type method was found to be more robust, but under predicted real failure probability at low loads. Introduction of a global failure threshold to account for the propagation dependency of failure was found to greatly improve the quality of failure prediction and the stability of the calibration process.

Introduction

Component failure is generally deemed to occur when a component has deformed due to gross yielding, such that it can no longer function as designed, or when fracture of the component has occurred. Failure due to fracture is of particular concern as, unlike gross yielding, there are often few external signs to indicate proximity to failure.

In order for designers to minimise the likelihood of such failures occurring, it is of paramount importance to have viable methods of predicting failure by fracture mechanisms which can be incorporated into structural integrity assessment methodologies. Currently, the majority of assessment methods are based on single parameter fracture mechanics, in particular the stress intensity factor (SIF) K . In general, it is assumed that for a body containing a defect (i.e. a macro scale crack), failure will occur when K for that defect is equal to K_{1C} , the material fracture toughness. This is justified based on the assumption that K controls the magnitude of the stress field in the near-crack region. In general this is a valid assumption as long as yielding in the near crack region is minimal.

Single parameter methods may be used as a deterministic criterion for failure, or incorporated into probabilistic methods, such as that proposed by Wallin [1]. An alternative fracture parameter, the J integral, was originally formulated for elastic materials [2] and in such cases J represents the energy release rate of crack propagation. It has been shown that J controls the near tip stress fields for elastic-plastic materials whose hardening behavior can be approximated by a power function of plastic strain [3,4]. However the applicability of the J integral in such cases is reliant on monotonic loading conditions; when yielding is followed by a reversal in load or where small strain assumptions are invalid, the physical meaning of J is no longer clear.

Experimental measurement of K_{1C} and J_{1C} are well known to exhibit strong dependencies on specimen geometry, e.g. [5]. This can be attributed to the fact that assuming near tip stresses are controlled primarily by J or K requires a degree of self-similarity between the near-tip stress fields

in differing geometries. In cases where levels of constraint are profoundly different or where a combination of applied and residual stresses exist, this is no longer the case. The theory of single parameter fracture mechanics requires that a given value of J or K corresponds to two possible local stress field solutions - one for plane stress and one for plane strain. The use of so called two parameter methods such as J-Q or K-T theory attempts to correct for deviations from the analytical field solutions by including a second parameter to characterise the level of constraint. However these approaches are also somewhat simplistic and lack the flexibility to accurately describe the possible range of both in-plane and out of plane constraint change.

An alternative approach is presented by 'local approach' methodologies, where global fracture probability is determined by examining the probability of failure nucleation in all elements of material volume meeting some criteria for inclusion into the failure process region. The advantage of such methods is that two highly dissimilar local stress fields with the same global failure probability can produce the same characterising value. Furthermore, such methods do not require a well defined macro-scale crack and so are applicable to a wider range of geometries.

This paper aims to compare the suitability of a number of failure criteria for predicting fracture in two highly dissimilar geometries, manufactured from 2024 aluminium. Two local approach methods are compared with J integral calculations and the relative merits of each methodology are discussed and compared.

Fracture criteria considered

J integral

The J integral, as given in [2] is expressed as follows

$$J = \int_{\Gamma} \left(W \delta_{ij} - \sigma_{ij} \cdot \frac{\partial u_j}{\partial x_i} \right) n_i ds \quad (1)$$

Where Γ is a closed contour surrounding the crack tip and n is the outward normal to Γ , u is the displacement vector and W is strain energy density and δ_{ij} is the Kroneker delta. In the context of elastic plastic materials, J is taken to be representative of the intensity of the stress field at the crack tip [3,4] .

Local approach – stress based methods

The well known Beremin model for cleavage fracture [6] states that the failure probability of any small element is a function of the maximum principal stress in that element. The model assumes that growth of an individual flaw obeys Griffith theory and that propagation of a single flaw leads to global failure. A probabilistic element is introduced by assuming a distribution of flaw sizes, with the appropriate flaw size/principal stress combination required to instigate failure,

$$Pf = 1 - \exp \left(- \left(\frac{\sigma_w - \sigma_m}{\sigma_0 - \sigma_m} \right)^m \right) \quad (2)$$

where σ_w , often termed the 'Weibull stress' is given by

$$\sigma_w = \left(\int_V \sigma_3^m \frac{dV}{V_0} \right)^{1/m} \quad (3)$$

with σ_3 denoting the maximum tensile principal stress, V the volume of material assumed to be contributing to fracture and V_0 a normalising volume. In this work, following [7], V is taken to be all areas actively yielding at the load level of interest. The values of m , σ_m and σ_0 in equations 2 and 3 are most commonly found by calibration to experimental data, e.g. [8].

The Beremin model was conceived to predict brittle fracture in steels, usually assumed to occur by means of inter- or trans-granular cleavage, nucleated at fractured inclusion particles and is not intended for cases where failure occurs by ductile mechanisms such as in aluminium. However, the experimental specimens analysed in this work exhibited approximately linear-elastic behaviour to failure, suggesting plasticity was well contained, and as such it was felt that the Beremin type model may still have some relevance.

An alternative definition of the 'Weibull stress' of equation 3 is also employed in this work, substituting maximum principal stress for hydrostatic stress, σ_h . This follows the work of Bass and coworkers [9] who found that such a method, based on hydrostatic stress, showed response to changing levels of out of plane loading where the principal stress formulation did not.

Local approach - Dilatational strain energy density

The dilatational energy approach is based upon the assumption that failure of a small element of material is governed by volumetric change in the material, characterised by the dilatational strain energy density. This can be seen as a measure of the divergence of the local displacement field, which can only be tolerated to a point, before creation of internal voids or micro-cracking occurs.

Strain energy density has been proposed as a failure criterion by Sih [10] and used to predict fracture where high levels of plasticity occur [11,12]. Previously, strain energy has been used as a deterministic parameter - i.e. failure occurs when the level of strain energy density, at a point exceeds a critical value. It is proposed that a probabilistic approach, such as that given in [7], may be a more realistic model for material failure by better accounting for small scale variations such as local micro-cracks or inclusion particles.

The dilatational strain energy density, W_v , is defined by equation 4 [12]. Plastic strain components are ignored when calculating W_v . The assumption is made, therefore that plastic flow is incompressible. It then follows that only elastic strain components contribute to local volume change.

$$W_v = \frac{1}{3} \int_V \sigma_{ii} d\epsilon_{jj} \quad (4)$$

The integral of W_v is taken across some integration volume, V , representing all regions of material contributing to the overall probability of fracture. The resulting 'Weibull energy' W_w is then used as a characteristic parameter, representing the likelihood of fracture. In this case V is defined as all regions where the material is yielding and where W_v is greater than a minimum value, W_m . Therefore, it is assumed that plastic flow is necessary but not sufficient to cause failure and some minimal level of W_v must also be attained. This is expressed in equation 5.

$$\begin{aligned} W_v - W_m > 0 &\rightarrow \delta W_w = (W_v - W_m) \delta V \\ W_v - W_m < 0 &\rightarrow \delta W_w = 0 \end{aligned} \Rightarrow W_w = \int_V (W_v - W_m) dV \quad (5)$$

Summing the elemental failure probabilities, assuming local probability of failure to be proportional to W_v , gives equation 6.

$$Pf = 1 - \exp\left(-\frac{W_w}{W_0}\right) \quad (6)$$

It can be seen from equations 5 and 6 that two parameters require calibration from experimental data, the threshold parameter W_m and normalizing parameter W_0 .

Experimental data

To investigate the applicability of the discussed approaches to predict fracture for any general geometry/load type, it was necessary to obtain failure data for a variety of specimen types. Two classes of geometry were selected for investigation in this work - single edge notched bend (SENB) and dual edge notched tension (DENT), as illustrated in figures 1 and 2. All specimens were made from 2024 series aluminium.

In the case of the DENT specimens, loading to failure occurred in the Y direction as shown in figure 1, with varying degrees of preload (0-90kN) applied in the X direction, via the loading apparatus also illustrated in figure 1. All SENB specimens were loaded in 3-point bending as illustrated in figure 2. Specimens were tested with crack lengths varying from $a=10.5\text{mm}$ to $a=19.0\text{mm}$. Notches were introduced into both specimens by means of wire electro-discharge machining (EDM) with notch tip radii of approximately 0.1mm. In the SENB specimens, this was followed by fatigue pre-cracking prior to loading to failure.

All specimens were loaded to failure at room temperature at a load line displacement rate of 0.2mm/min. In the case of the DENT specimens, preload was applied and then held at the desired level while the load in the Y direction was increased until failure occurred. In all cases, global behaviour was approximately linear to failure.

Analysis of the fracture surfaces using electron microscopy showed failure in all cases to be tensile type, i.e. failure occurring by strain localisation and internal necking between voids.

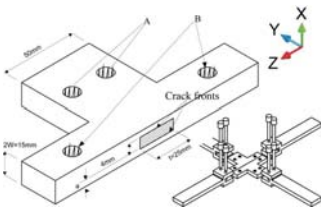


Figure 1: Schematic of DENT specimens. Diagram shows half a specimen, (symmetry in the Y axis), and the loading apparatus

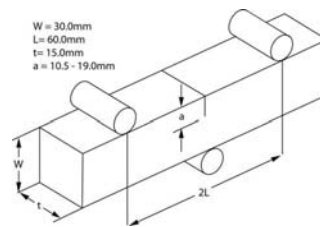


Figure 2: SENB specimen geometry, showing location of load rollers for 3 point bend loading.

Results

Finite Element modelling

In order to calibrate and calculate the discussed failure parameters, detailed stress field data is needed. In this work, component stress/strain fields were modelled using the ABAQUS finite element code, version 6.7-1. A high degree of mesh refinement was used in the near crack regions to capture the high stress gradients, with near tip element sizes of approximately $50\mu\text{m}$. As calculation of W_v and σ_w required integration across element volumes, quadratic element formulations were used such that each quadrilateral element had 8 gauss points and 20 nodes. Using specimen symmetry, 1/4 and 1/8 models were used for the SENB and DENT geometries respectively. A bilinear material model was used with kinematic hardening. A number of analyses were also carried out using isotropic hardening and the impact on results was found to be minimal.

Calculation of J was carried out using an inbuilt routine in the ABAQUS FE code, all other parameters were calculated using an in house post processor routine.

Calibration and prediction methods

In order to correctly calibrate local approach methods, it is desirable to have at least two data sets, corresponding to high and low constraint cases. This is discussed by Ruggieri and coworkers in the context of the Beremin model [7] who noted that there may exist an infinite number of sets of calibrated parameters which fit a given set of data equally well - a problem arising from the self similarity of local stress fields in a given specimen type. By calibrating to multiple specimen geometries, a single set of parameters for a given material may be found. In this case, the available data consists of a small number of failure values for each specimen/load type, which did not permit reliable fitting to a single specimen geometry and load regime.

To circumvent this problem, DENT type specimen failure data for all preload levels were combined and ranked by the failure parameter in question (i.e. W_w or σ_w), with failure probabilities assigned using the following ranking approximation

$$Pf = \frac{i - 0.5}{N} \quad (7)$$

where i is the position in the ranked data and N is the total number of samples. The Beremin fit parameters - m , σ_0 and σ_m - were obtained from a maximum likelihood estimate fit to the data. The parameters W_0 and W_m in equations 5 and 6 were obtained by varying the value of W_m and using a the method of least squares to determine the value of W_0 , the best fitting combination was determined by maximising the value of the coefficient of determination, R^2 , for the data fit.

The adopted approach to data fitting was to calibrate parameters to the data set obtained from the DENT specimens and use the resultant values to predict failure of the SENB specimens. Upon calibration of the parameters W_0 and W_m it was noted that the relationship between Pf as given by equation 7 and W_w was not well characterised at low values of Pf by equation 6, the fit was greatly improved by addition of a 'global' threshold value, W_T , such that the failure probability was given by

$$Pf = 1 - \exp\left(-\frac{W_w - W_T}{W_0}\right) \quad (8)$$

The global threshold can be interpreted physically as a parameter controlling the propagation of fracture, such that a minimum value of W_w must be attained before locally nucleated voids or micro cracks can be propagated to global failure.

Calculated J integral values at failure for both specimen types are illustrated in figure 3, where J was taken to be the maximum calculated value along the crack front at the failure load. Weibull distributions were fitted to the SENB and DENT data sets, with the resultant exponent and normalizing values given in figure 3.

Predicted failure envelopes (5% and 95% failure probability) for the SENB specimens, based on equations 2 and 3, are displayed in figure 4 and the predictions from equations 6 and 8 (5%, 50% and 95% failure probability) are given in figure 5. Due to the limited data available for calibration, data fits were also carried out on the entire data set, i.e. both the SENB and DENT specimens, in order to judge the inherent capability of each of the failure models to fit a wide range of failure situations. Predicted failure envelopes for the SENB specimens, following calibration to the entire data set are given in figures 6 and 7, with lines corresponding to 5%, 50% and 95% failure probabilities.

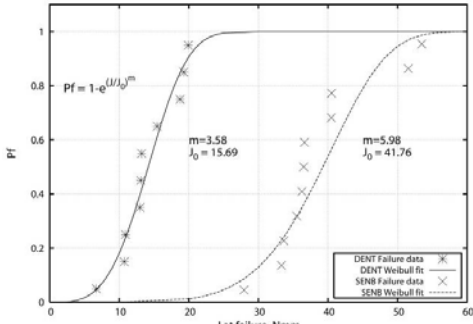


Figure 3: Ranked failure probability estimate plotted against J integral at failure for SENB and DENT type specimens

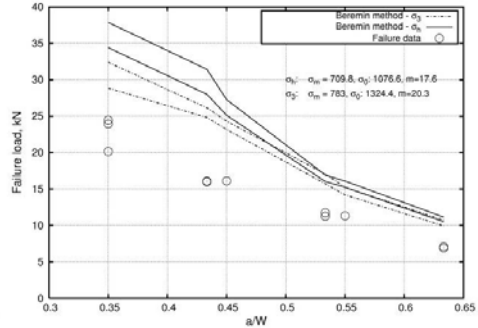


Figure 4: SENB failure data and predicted failure envelopes from equation (2), based on fit to DENT data

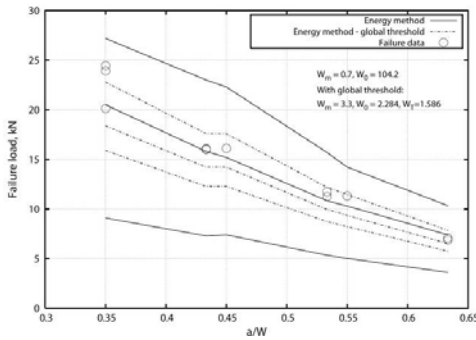


Figure 5: SENB failure data and predicted failure envelopes from equations 6 and 8, based on fit to DENT data

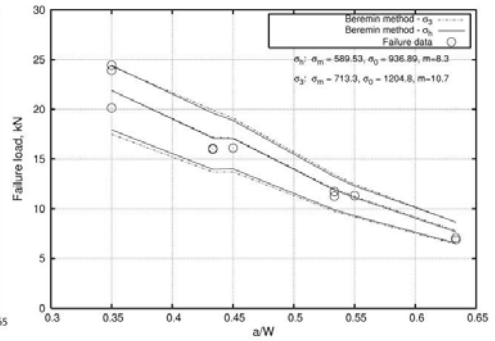


Figure 6: SENB failure data and predicted failure envelopes from equation (2), based on fit to DENT and SENB data

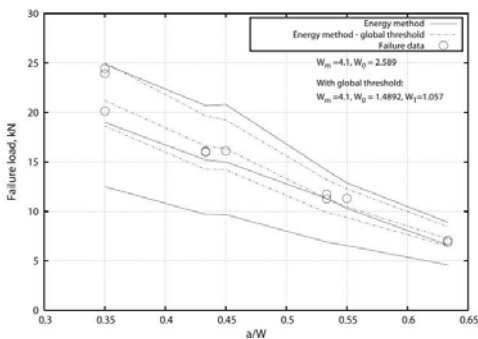


Figure 7: SENB failure data and predicted failure envelopes from equations 6 and 8, based on fit to DENT and SENB data

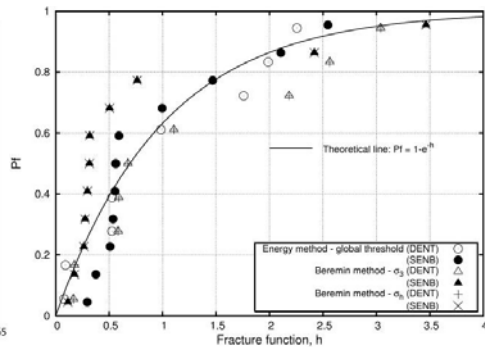


Figure 8: Failure functions from equations 2 and 8, calibrated to SENB and DENT data sets, plotted against failure probability.

Discussion of Results

From results illustrated in figure 3, it is clear that the J integral is non-transferable between the geometries used here with no overlap between the two sets of failure data. Therefore, it would seem that J cannot be viewed as a valid general fracture parameter in its standard form. Based on fitting to the DENT data set, it can be seen from figure 4 that both models based on the Beremin method significantly over-predict the failure loads for the SENB specimens. In the case of the energy method, figure 5 shows that equation 6 places all failure data points within the 5%-95% failure probability envelope, although the 5% probability line seems overly pessimistic. The addition of a global threshold parameter significantly increases the level of the 5% line, providing good agreement with the failure data, although 2 failure loads for SENB specimens with crack length 10.5mm ($a/w = 0.35$) lie above the 95% limit, indicating the model fit could still be improved.

When the SENB data are also included in the calibration process, the results of the Beremin type models are drastically improved, as shown in figure 6, with a significant drop in the value of the Weibull exponent m . Results for the dilatation energy method (figure 7) are not significantly altered by the inclusion of the SENB data, although the width of the 5-95% envelope is decreased for the method of equation 6, and the upper threshold of equation 8 is raised to include the two previously excluded points. In all cases for figures 6 and 7, the 50% probability line runs approximately through the centre of the available data, indicating no undue bias towards either end of the probability spectrum.

To better compare the inherent quality of the fits provided by equations 2 and 8 the 'fracture function', as given by equations 9 and 10, was plotted for each of the 3 methods, based on calibration to both data sets.

$$h(W_v) = \frac{W_v - W_T}{W_0} \quad (9)$$

$$h(\sigma_w) = \left(\frac{\sigma_w - \sigma_m}{\sigma_0 - \sigma_m} \right)^m \quad (10)$$

It can be seen from figure 8 that there is still clear separation between the two data sets when h is determined from equation 10, whereas equation 9 brings the two sets much closer together, as well as providing better agreement to the theoretical curve. It therefore appears that the formulation of equation 8 is better able to characterise failure for the considered material than the more traditional Beremin model. As dilatational energy as expressed in equation 4 is proportional to σ_h^2 it is perhaps surprising that the results of the energy approach should differ from those due to equation 2 based on hydrostatic stress. This result may suggest that the power formulation of equations 2 and 3 (arising from an assumed distribution of inclusion particle sizes in ferritic steels) is unsuitable for aluminium alloys where a 'weakest link' model of failure seems inappropriate, given the nature of the void growth mechanism leading to fracture. Similar trends were noted for steels where some ductility occurs prior to failure by Bordet et al [13].

Conclusions

The results of the study described have produced the following conclusions:

1. Based on the results here, the J integral in its standard formulation is not transferable between geometries where constraint or load type varies significantly.

2. Based on calibration to 1 specimen type, local approach methods based on the Beremin model were unable to accurately predict failure in another specimen type, although when a larger calibration data set was employed accurate predictions were obtained. A sizable variation in calibrated Weibull exponent was noted, indicating a high degree of sensitivity to the data used for calibration and the importance of large data sets for accurate determination of the values of the distribution constants, m , σ_0 and σ_m .
3. Calibration of the local approach method based on dilatation strain energy was found to exhibit a reduced sensitivity to smaller data sets, producing good prediction of the failure of SENB specimens when calibrated to biaxial DENT specimens although estimates of failure probability at low loads were felt to under predict failure load levels corresponding to low failure probabilities. Calibration to both data sets had an sizeable effect on the calibration constants, W_v and W_0 , although the predicted failure envelope was not significantly affected
4. A modification of the energy based approach to include a ‘global’ failure threshold, W_T , was found to greatly improve agreement with experimental data, especially at low applied loads. Good prediction of SENB specimen failure was obtained from calibration to the DENT data. Calibrated values were altered somewhat by inclusion of the SENB data set to the fitting process, but less significantly than for the energy method without W_T of the Beremin method. This method appears to be capable of characterizing failure in the 2024 aluminium material investigated here, although further investigation is needed to determine whether this is due to the use of dilatation energy as a characterising field quantity or the formulation of the probability distribution.
5. All three local approach variants were able to characterize the two data sets analysed in terms of a ‘fracture function’, although there was appreciable separation between the two specimen types for the Beremin model, suggesting the physical grounding of this approach is unsuitable for the material studied.

References

- [1] K. Wallin, *Engineering fracture mechanics* 19(6): 1085-1093 (1984)
- [2] J.R. Rice, *Journal of applied mechanics*, 35: 379-386 (1968)
- [3] J.R Rice and G.F Rosengren, *Journal of Mech. and Phys. of solids*, 16: 1-12, (1968)
- [4] J.W. Hutchinson, *Journal of Mech. and Phys. of solids* 16: 13-31, (1968)
- [5] S. Mahmoud and K. Lease, *Engineering fracture mechanics*, 70: 443-452 (2003).
- [6] S. Hadidi-Moud et al., *Fat. & Frac. of Eng. Materials & Structures*, 27:931-942, (2004).
- [7] F.M. Beremin, *Metall. Trans. A*, 14A: 2277-2287, (1983).
- [8] C. Ruggieri, X. Gao and R.H. Dodds, *International Journal of fracture*, 92: 175-200, (1998).
- [9] P.T. Williams, B.R. Bass *et. al.*, *Nuclear engineering and design*, 188: 259-288, (1999)
- [10] G.C. Sih and B. Macdonald, *Engineering fracture mechanics*, 6: 361-386, (1974).
- [11] G.C. Sih and E. Madenci, *Engineering fracture mechanics*, 18(3): 667-677, (1983).
- [12] C.L Chow and Jilin Xu, *International Journal of fracture*, 28:17-28, (1985).
- [13] S.R. Bordet, A.D Karstensen *et. al.*, *Engineering fracture mechanics*, 72(3): 435-452 (2005)